Article

Crystallization and Investigation of the Structural and Optical Properties of Ce^{3+}-Doped Y$_{3-x}$Ca$_x$Al$_{5-y}$Si$_y$O$_{12}$ Single Crystalline Film Phosphors

Vitalii Gorbenko [1,*], Tetiana Zorenko [1], Sandra Witkiewicz-Łukaszek [1], Anna Shakhno [1], Andres Osvet [2], Miroslaw Batentschuk [2], Aleksandr Fedorov [3] and Yuriy Zorenko [1,*]

[1] Institute of Physics, Kazimierz Wielki University in Bydgoszcz, 85090 Bydgoszcz, Poland; tetiana.zorenko@ukw.edu.pl (T.Z.); s-witkiewicz@wp.pl (S.W.-Ł.); annshakhno@gmail.com (A.S.)
[2] Department of Materials Science and Engineering VI, Institute of Materials for Electronics and Energy Technology (i-MEET), University of Erlangen-Nürnberg, 91058 Erlangen, Germany; andres.osvet@fau.de (A.O.); miroslaw.batentschuk@fau.de (M.B.)
[3] SSI Institute for Single Crystals, National Academy of Sciences of Ukraine, 61178 Kharkiv, Ukraine; fedorov@xyz.ua
* Correspondence: gorbenko@ukw.edu.pl (V.G.); zorenko@ukw.edu.pl (Y.Z.)

Abstract: This work is devoted to the crystallization and investigation of the optical properties of single crystalline films (SCFs) of Ce^{3+}-doped Y$_{3-x}$Ca$_x$Al$_{5-y}$Si$_y$O$_{12}$ garnet, where the content of Ca^{2+} and Si^{4+} cations varied in the x = 0.13–0.52 and y = 0.065–0.5 ranges, respectively. The SCF samples were grown using the liquid phase epitaxy technique onto Y$_3$Al$_5$O$_{12}$ substrates from the melt solution with equimolar Ca and Si content using PbO-B$_2$O$_3$ flux. However, the Ca and Si concentration in Y$_{3-x}$Ca$_x$Al$_{5-y}$Si$_y$O$_{12}$:Ce SCFs is not equal: the Ca^{2+} content was systematically larger than that of Si^{4+}, and the Ca^{2+} excess is compensated for by the Ce^{4+} ion formation. The absorption, scintillation, and luminescent properties of Y$_{3-x}$Ca$_x$Al$_{5-y}$Si$_y$O$_{12}$:Ce SCFs with different Ca/Si concentrations were investigated and compared with the sample of YAG:Ce SCF. Due to the creation of Ce^{4+} ions, the as-grown Y$_{3-x}$Ca$_x$Al$_{5-y}$Si$_y$O$_{12}$:Ce SCFs show relatively low light yield (LY) under α–particle excitation but a fast scintillation response with a decay time in the ns range. After SCF annealing in the reducing (N$_2$ + H$_2$) atmosphere at T > 1000 °C, the recharging of Ce^{4+}→Ce^{3+} ions occurs. Furthermore, the samples annealed at 1300 °C SCF possess an LY of about 40% in comparison with the reference YAG:Ce SCF and scintillation decay kinetics much closer to that of the SCF counterpart. Due to Ca^{2+} and Si^{4+} alloying, the Ce^{3+} emission spectra in Y$_{3-x}$Ca$_x$Al$_{5-y}$Si$_y$O$_{12}$ SCFs are extended to the red range in comparison with the spectra of YAG:Ce SCF. Such an extension is caused by the Ce^{3+} multicenter formation at the substitutions of both Y^{3+} and Ca^{2+} dodecahedral positions in the hosts of these mixed garnets.

Keywords: liquid phase epitaxy; single crystalline films; YAG garnet; Ca^{2+} and Si^{4+} alloying; Ce^{3+} dopant

1. Introduction

Currently, white light emitting diodes (WLEDs) are displacing traditional light sources due to their high luminous efficiency, energy saving ability, long lifetime, and environmental friendliness [1]. At present, a conventional WLED in the so-called volume casting approach (VCA) is based on the blue LED chip and yellow emitting Y$_3$Al$_5$O$_{12}$:Ce (YAG:Ce) powder phosphor embedded in the epoxy resin [2]. However, YAG:Ce ceramics or crystal plates also accessible for light conversion, producing high power WLEDs in the planar casting approach (PCA) [3–12]. Ceramic phosphors based on the different kinds of Ce^{3+}-doped Ln$_3$Al$_5$O$_{12}$ garnets have also been developed for PCA application [4–12].

The {Y}$_3$[Al]$_2$(Al)$_3$O$_{12}$ garnet structure is characterized by a great flexibility, which allows for the relatively simple replacing of cations in the dodecahedral { }, octahedral [ ], and

tetrahedral ( ) sites. For this reason, it is possible to modify the content of this garnet for optimization of the Ce^{3+} spectroscopic properties for the demands of applications in WLEDs. Recently, a new class of garnet phosphors based on Ce^{3+}-doped $A_3B_2C_3O_{12}$ (A = Ca, R = Y, Lu; B = Mg, Sc, Al, Ga; C = Ga, Al, Si) silicate garnets has been proposed for creation of high-power WLEDs [13–20]. The ceramics of Ce^{3+}-doped $\{Ca_2R\}[B_{2-x} C_x](Si_{3-y}C_y)O_{12}$:Ce (R = Y, Lu; B = Sc, Ga; C = Ga, Al; x, y = 0–1) and $\{Ca_2Y\}[Sc]_2(Si)_3O_{12}$:Ce garnets were crystallized for use as LED converters and their luminescent properties were investigated as well [21,22]. The $\{Ca_3\}[Sc]_2(Si)_3O_{12}$:Ce and $\{Ca_2Y\}[Sc]_2(Si)_3O_{12}$:Ce garnets were also obtained in the form of single crystalline films (SCFs) using the liquid phase epitaxy (LPE) growth method for application as blue LED converters and laser media [23–25]. Furthermore, these two types of garnets and other garnet compounds of this family are currently considered as prospective materials for the creation of new advanced SCF scintillators, cathodoluminescent screens, and solar cells [23,24].

However, many questions in studying the luminescent properties of mixed silicate garnets are still open today due to the lack of single crystal samples grown by traditional methods, such as Czochralski, Bridgman, and micro-pulling-down techniques, for basic investigations and practical applications. First, it is interesting to investigate the influence of the Ca^{2+} -Si^{4+} pair in the YAG host with regards to the creation of different kinds of Ce^{3+}-based centers due to the different local disorder induced by doping with +2 and +4 charged cations. Another important task of these investigations is connected with the estimation of the real potential of luminescent materials based on different kinds of crystals and ceramics of Ca^{2+}-Si^{4+}-based mixed garnets for different optoelectronic applications, including photovoltaic devices, LED convertors, and scintillators.

In this work, we present the results on the crystallization and investigation of the structural and optical properties of phosphors based on the SCFs of Ce^{3+}-doped $Y_{3-x}Ca_xAl_{5-y}Si_yO_{12}$ garnet, where x = 0.13–0.52 and y = 0.065–0.5. We hope that the results of this pilot research will be useful for the development of luminescent materials for white LED converters, scintillators, cathodoluminescent screens, and other optoelectronic devices based on the epitaxial structures of Ca^{2+}-Si^{4+}-containing garnets, grown using the LPE method on doped or undoped substrates of garnet compounds.

2. Growth of $Y_{3-x}Ca_xAl_{5-y}Si_yO_{12}$ SCF by LPE Method

Five sets of optically perfect $Y_{3-x}Ca_xAl_{5-y}Si_yO_{12}$:Ce SCF samples were crystallized using the LPE method on YAG substrates with an orientation close to (110) from the super cooling melt solution containing nominal equimolar (x = y) Ca and Si content in the 0.5–2 range (Figure 1). The melt of PbO-B_2O_3 (12:1) oxides was used as a flux in the LPE growth procedure. The PbO, B_2O_3, Y_2O_3, Al_2O_3, CaO, SiO_2, and CeO_2 raw materials were of 4N purity.

The real composition of SCF samples was determined using a JEOL JSM-820 electronic microscope (Tokyo, Japan), equipped with IXRF 500 and LN2 Eumex EDX detectors, and is presented in Table 1. The measurements were performed in the 5–10 points of the SCF sample with subsequent averaging of results for improving the accuracy of content determination to the 0.001–0.003 at.% level depending on the cation type.

From the microanalysis of the real content of the SCF samples (Table 1), we also found the Ca^{2+} and Si^{4+} segregation coefficients in $Y_{3-x}Ca_xAl_{5-y}Si_yO_{12}$:Ce SCF samples at nominal Ca (x) and Si (y) content in the melt solution in the 0.5–2 range (Figure 2). As can be seen from this figure, the variation in the ratio between the Y/Ca–Si/Al content in the melt solution and the SCF growth temperature T_g leads to a noticeable change of their segregation coefficients. Namely, the Ca^{2+} and Si^{4+} segregation coefficients are nonlinearly varied in the 0.17–0.27 and 0.065–0.25 ranges, respectively, when the nominal Ca (x) and Si (y) content in the melt solution was changed from 0.5 to 2.0 and the respective growth temperature T_g was changed within the 960–1020 °C range. The segregation coefficient of Ce^{3+} ions in the mentioned mixed garnet hosts was very low and equal to around 0.025–0.0325.
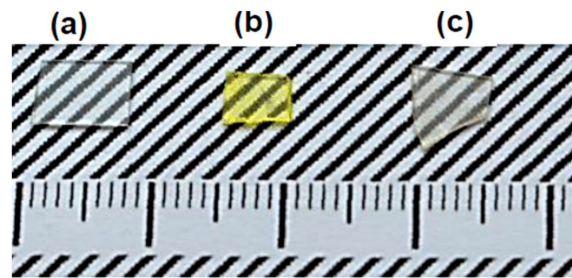
Figure 1. Photo of YAG substrate (**a**), as-grown $Y_{2.95}Ce_{0.05}Al_5O_{12}$:Ce (**b**), and $Y_{2.43}Ca_{0.52}Ce_{0.05}Al_{4.5}Si_{0.5}O_{12}$ (**c**) SCFs (see also Table 1).
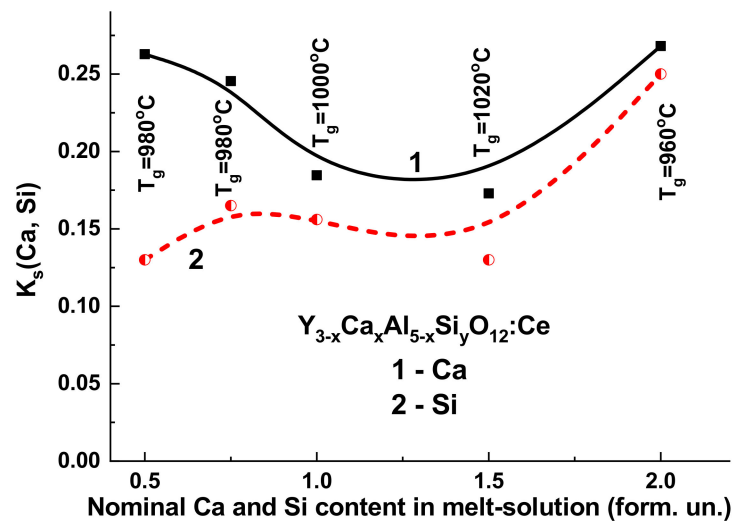

Figure 2. Dependence of the segregation coefficient of Ca^{2+} (1) and Si^{4+} (2) ions at growth of $Y_{3-x}Ca_xAl_{5-y}Si_yO_{12}$:Ce SCFs onto YAG substrates when changing nominal Ca (x) and Si (y) content in melt solution in the 0.5–2 range and SCF growth temperature in the 960–1020 °C range (see Table 1).

Table 1. Nominal (in melt solution) and real (in film) content of $Y_{3-x}Ca_xAl_{5-y}Si_yO_{12}$ and YAG: Ce SCFs, LPE grown on YAG substrates by using PbO-B_2O_3 flux.

No	Nominal SCF Content	Real SCF Content
R	$Y_3Al_5O_{12}$:Ce	$Y_{2.95}Ce_{0.05}Al_5O_{12}$:Ce
1	$Y_{2.5}Ca_{0.5}Al_{4.5}Si_{0.5}O_{12}$:Ce	$Y_{2.825}Ca_{0.13}Ce_{0.065}Al_{4.935}Si_{0.065}O_{12}$
2	$Y_{2.25}Ca_{0.75}Al_{4.25}Si_{0.75}O_{12}$:Ce	$Y_{2.765}Ca_{0.18}Ce_{0.055}Al_{4.875}Si_{0.125}O_{12}$
3	$Y_2CaAl_4SiO_{12}$:Ce	$Y_{2.77}Ca_{0.185}Ce_{0.045}Al_{4.845}Si_{0.155}O_{12}$
4	$Y_{1.5}Ca_{1.5}Al_{3.5}Si_{1.5}O_{12}$:Ce	$Y_{2.685}Ca_{0.26}Ce_{0.055}Al_{4.785}Si_{0.195}O_{12}$
5	$YCa_2Al_3Si_2O_{12}$:Ce	$Y_{2.43}Ca_{0.52}Ce_{0.05}Al_{4.5}Si_{0.5}O_{12}$

It is important to note here that the real Ca and Si content in SCFs is not equal at the equimolar concentration of these ions in the melt solution, especially at a low (x = 0.13–0.18 and y = 0.065–0.12) content of these ions (Table 1). As can be seen from this table, the Ca^{2+} concentration was systematically larger than that of the Si^{4+}. This means that for local charge compensation, the other 4+ ion states can be created—for instance, Ce^{4+} ions or Pb^{4+} flux related dopants—or local charge compensation can occur by means of formation of the oxygen vacancies. We can predict here both types of charge compensation of Ca^{2+} excess in the $Y_{3-x}Ca_xAl_{5-y}Si_yO_{12}$ SCFs: the predominant formation of Ce^{4+} and Pb^{4+} states at the mentioned low Ca-Si content and the preferable formation of oxygen vacancies at a large Ca-Si concentration (Figure 2).

The XRD measurements were used for the characterization of the structural quality of $Y_{3-x}Ca_xAl_{5-y}Si_yO_{12}$ SCFs with different content x of Ca and Si cations, grown onto

the YAG substrate with the (110) orientation and a lattice constant of 12.0069 Å (Figure 3). From the respective XRD patterns of the $Y_{2.43}Ca_{0.52}Ce_{0.05}Al_{4.5}Si_{0.5}O_{12}$ SCF sample, the difference between the lattice constants of the YAG substrate and film $\Delta a = (a_{SCF} - a_{sub})/a_{sub} \times 100\%$ was estimated, which was equal to 0.53% (Figure 3). Additionally, for this garnet composition, the lattice constant was calculated, which equals 12.0705 Å (Figure 3).
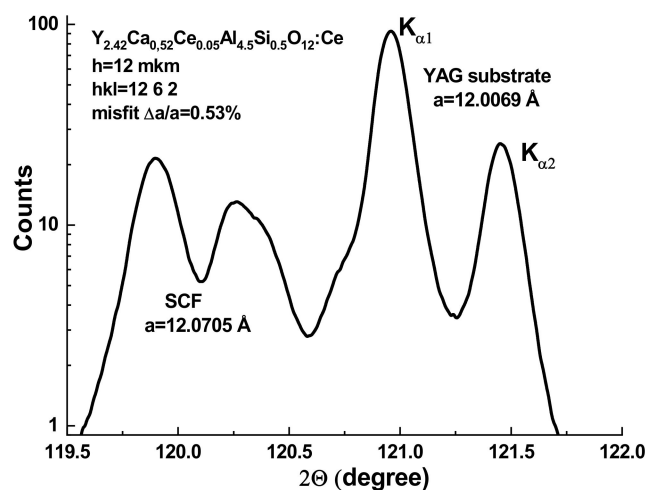

Figure 3. XRD patterns of (1262) planes of $Y_{2.43}Ca_{0.52}Ce_{0.05}Al_{4.5}Si_{0.5}O_{12}$ SCF, LPE grown onto YAG substrate from melt solution with $YCa_2Al_3Si_2O_{12}$:Ce nominal content (see Table 1).

3. Optical Properties of $Y_{3-x}Ca_xAl_{5-y}Si_yO_{12}$ SCF

For the characterization of the optical properties of the Ce^{3+}-doped $Y_{3-x}Ca_xAl_{5-y}Si_yO_{12}$:Ce SCFs, the absorption spectra (Figure 4), cathodoluminescence (CL) spectra (Figure 5), photoluminescence (PL) spectra (Figure 6), PL excitation spectra (Figure 7), and PL decay kinetics (Figure 8 and Table 2) were used. We also performed the measurement of the scintillation decay kinetics and photoelectron light yield for these SCF samples under excitation by α–particles (Table 3 and Figure 9). The absorption, luminescent, and scintillation properties of $Y_{3-x}Ca_xAl_{5-y}Si_yO_{12}$:Ce SCFs with different Ca/Si content were compared with the properties of the reference YAG:Ce SCF sample (Tables 2 and 3). The absorption spectra of the SCFs were measured using a Jasco V730 spectrophotometer (Oklahoma, OK, USA). The PL emission and excitation spectra as well as the PL decay kinetics of the SCFs were measured using an Edinburg Instrument FS5 spectrofluorometer (Livingston, UK).

The CL spectra were recorded at room temperature (RT) with a scanning electron microscope JEOL JSM-820, which was also equipped with a spectrometer Ocean Electronics and a TE-cooled CCD detector that worked in the 200–925 nm range. The scintillation LY with a shaping time of 12 s and decay kinetics under irradiation by α-particles of Pu^{239} (5.15 MeV) source were measured using a setup based on the Hamamatsu H6521 PMP (Hamamatsu, Japan), multichannel analyzer, and digital TDS3052 oscilloscope (Colby, UK). All optical measurements were performed at room temperature.

3.1. Absorption Spectra

The absorption spectra of $Y_{3-x}Ca_xAl_{5-y}Si_yO_{12}$:Ce SCFs with different Ca and Si content in the x = 0.13–0.52 and y = 0.065–0.5 ranges, respectively, are shown in Figure 4 in comparison to the YAG:Ce counterpart's spectra. In the YAG:Ce garnet, the measured absorption bands E_1 and E_2 peaked at 460 and 340 nm, respectively, and correspond to the Ce^{3+} ion's $4f^1(^2F_{5/2}) \rightarrow 5d$ (^2E) transitions in the garnet host (Figure 4, curve 1). The Ca^{2+} and Si^{4+} alloying in YAG SCFs in the mentioned concentration ranges leads to the strong decrease in the intensity of the Ce^{3+} absorption bands. Furthermore, in the $Y_{3-x}Ca_xAl_{5-y}Si_yO_{12}$:Ce SCF samples, these bands are almost dissipated (Figure 4). On the other hand, the wide absorption bands that peaked at approximately 250 nm dominate

in the spectra of these SCFs (Figure 4, curves 2–3). The nature of these bands is related to the $O^{2-} \rightarrow Ce^{4+}$ charge transfer transitions (CTT) [23]. These CTT bands at similar positions are also observed in Mg^{2+} and Ca^{2+}-doped $Lu_3Al_5O_{12}$:Ce and $Gd_3Ga_3Al_2O_{12}$:Ce garnets [26,27]. This means that in the as-grown $Y_{3-x}Ca_xAl_{5-y}Si_yO_{12}$:Ce SCFs, the main charge state of cerium ions is the Ce^{4+} valence states. It is worth noting here that the onset of $O^{2-} \rightarrow Ce^{4+}$ CTT in these SCFs can even be shifted up to 400 nm, leading to a significant overlap with the E_2 absorption bands of Ce^{3+} ions.

Apart from the Ce^{3+} and $O^{2-} \rightarrow Ce^{4+}$ CTT-related bands, the bump around 260 nm is also observed in the absorption spectra of $Y_{3-x}Ca_xAl_{5-y}Si_yO_{12}$:Ce SCFs grown from the flux based on PbO. This band is related to the $^1S_0 \rightarrow ^3P_1$ transitions of Pb^{2+} ions as the main flux contamination in the SCFs [28]. The similar band is observed at 262 nm in the YAG:Ce SCF (Figure 3, curve 1). Furthermore, the Ca-Si alloying also leads in the SCFs to the formation of a wide complex absorption band peaking in the 400–500 nm range. Within the frame of assumptions concerning Pb^{4+} ion formation for the charge compensation of Ca^{2+} excess in the SCF samples, we can attribute this complex band to the $O^{2-} \rightarrow Pb^{4+}$ and $Pb^{2+} \rightarrow Pb^{4+}$ CTTs. Such types of transitions are observed by Scott and Page in the absorption spectra of the YGG:Pb garnet [29].
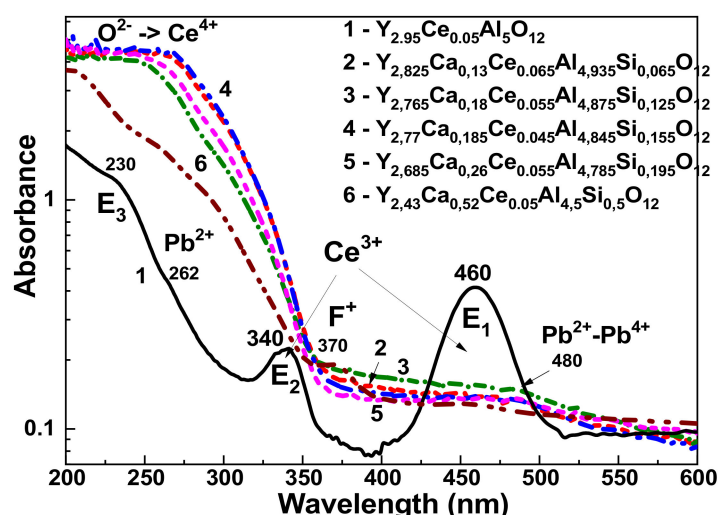

Figure 4. RT absorption spectra of $Y_{3-x}Ca_xAl_{5-y}Si_yO_{12}$:Ce SCFs in (log scale) with different Ca and Si content (2–6) in comparison with absorption spectra of YAG:Ce SCF (1).

The band peaking at 370 nm in the absorption spectra of the $Y_{2.43}Ca_{0.52}Ce_{0.05}Al_{4.5}Si_{0.5}O_{12}$ SCF is most probably related to the intrinsic 1A→1B transitions of the F^+ center [30]. This band also coincides with excitation band of the F^+ luminescence in $Y_{3-x}Ca_xAl_{5-y}Si_yO_{12}$:Ce SCFs (Figure 6b). The evidence of this characteristic absorption/excitation band confirms the presence of oxygen vacancy formation in Ca^{2+}-Si^{4+}-based SCFs even at the conditions of their low-temperature (below 1000 °C) growth in an oxygen-containing (air) atmosphere [23]. This also means that the charge compensation of Ca^{2+} excess in the CFs under study can also occur due to the formation of the charged oxygen vacancies.

3.2. Cathodoluminescence Spectra

The normalized RT CL spectra of the $Y_{3-x}Ca_xAl_{5-y}Si_yO_{12}$:Ce SCFs with different Ca and Si content in the x = 0.18–0.52 and 0.125–0.5 ranges, respectively, are displayed in Figure 4 in comparison to the YAG:Ce SCF counterpart. The $5d^1 \rightarrow 4f(^2F_{5/2;7/2})$ transitions of Ce^{3+} ion in these garnets correlate with the main luminescence band peaking at 533 nm in the YAG:Ce SCF (Figure 5, curves 1). Meanwhile, in comparison with the YAG:Ce, the position of these bands is strongly redshifted to 545–547 nm in $Y_{3-x}Ca_xAl_{5-y}Si_yO_{12}$:Ce SCFs (Figure 5, curves 3 and 4). It is important to note here that the Ce^{3+} emission bands

are notably broadened in these SCFs with respect to spectra of YAG:Ce SCFs. Particularly, the respective FWHM values of Ce^{3+} emission bands are equal to 0.465 eV in $Y_{2.43}Ca_{0.52}Ce_{0.05}Al_{4.5}Si_{0.5}O_{12}$ SCF and only 0.396 eV in YAG:Ce (Figure 5, curve 1). Such broadening of the Ce^{3+} emission band in Ca-Si-doped garnets can be related to increasing the electron–phonon interaction or/and with the formation of the Ce^{3+} multicenter in the dodecahedral position of these garnet hosts.
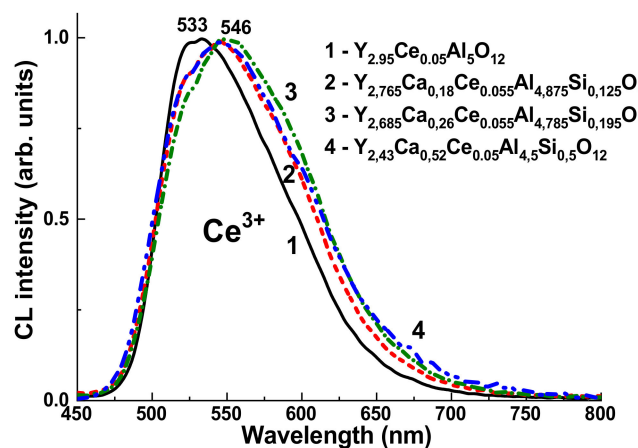

Figure 5. Normalized CL spectra at RT of $Y_{3-x}Ca_xAl_{5-y}Si_yO_{12}$:Ce SCFs with different Ca and Si content (2–4) in comparison with CL spectra of YAG:Ce SCF (1).

It is also worth noting that in all the SCFs under study, the luminescence of the Y_{Al} antisite defects [31] is not observed due to the low temperatures of their crystallization below 1000 °C. Only in the $Y_{2.43}Ca_{0.52}Ce_{0.05}Al_{4.5}Si_{0.5}O_{12}$ SCF sample is the very low intensity band peaking at 400 nm observed (not shown in Figure 5). This band can be associated with the luminescence of F^+ centers in this garnet. The investigation of the PL emission/ excitation spectra, as well as the PL decay kinetics of F^+ centers, provided additional validation of this conclusion (Figures 6b–8b).

3.3. Photoluminescence Spectra

Under excitation at the E_1 Ce^{3+} absorption band at 340 nm, the PL spectra of $Y_{3-x}Ca_x$ $Al_{5-y}Si_yO_{12}$:Ce SCFs exhibit luminescence in double wide bands, which is related to the $5d^1 \to 4f(^2F_{5/2,7/2})$ transitions of Ce^{3+} ions (Figure 6a). Namely, these bands are peaked at 520 and 553 nm for $Y_{2.765}Ca_{0.18}Ce_{0.05\,5}Al_{4.875}Si_{0.125}O_{12}$ SCFs and at 537 and 570 nm for the $Y_{2.43}Ca_{0.52}Ce_{0.05}Al_{4.5}Si_{0.5}O_{12}$ SCF. The low intensity of this luminescence is caused by a very low concentration of Ce^{3+} ions in the as-grown SCFs due to the preferable formation of Ce^{4+} ions in them (Figure 4). Furthermore, as opposed to the CL spectra, the position of PL emission bands and their FHWM in $Y_{3-x}Ca_xAl_{5-y}Si_yO_{12}$:Ce SCFs under excitation at 340 nm shows more complicated dependence on the x, y values of Ca^{2+}-Si^{4+} content. Namely, the PL spectra of the $Y_{2.765}Ca_{0.18}$ $Ce_{0.055}Al_{4.875}Si_{0.125}O_{12}$ SCF are significantly (11 nm) redshifted and notably broadened (FWHM = 0.479 eV) with respect to the spectra of the YAG:Ce SCF (FWHM = 0.457 eV), when the PL spectrum of Ce^{3+} in the $Y_{2.43}Ca_{0.52}Ce_{0.05}Al_{4.5}Si_{0.5}O_{12}$ SCF shows a small (5 nm) blueshift and practically the same FWHM = 0.458 eV as that in the YAG:Ce SCF (Figure 6a). Such phenomena of the PL spectra of $Y_{3-x}Ca_xAl_{5-y}Si_yO_{12}$:Ce SCFs under a fixed excitation wavelength also indicate the complicated character of Ce^{3+} center formation in these garnets and influence at least of two factors in this process.

The luminescence of F^+ centers in the band peaking at 397 nm is also observed in the $Y_{2.43}Ca_{0.52}$ $Ce_{0.05}Al_{4.5}Si_{0.5}O_{12}$ SCF sample under excitation at 370 nm in the respective absorption band of this center (Figure 6b). Another low intensity band peaking at 605 nm

can be related to the dimmer or more complicated centers, based on the charged oxygen vacancies in the YAG host (Figure 6b) (see [32] for details).

The excitation spectra of the Ce^{3+} luminescence in $Y_{3-x}Ca_xAl_{5-y}Si_yO_{12}$:Ce SCFs exhibit two bands peaking in the 454–457.5 nm and 340–344 nm ranges, respectively, associated with the $4f(^2F_{5/2}) \rightarrow 5d^{1,2}$ transitions of Ce^{3+} ions and corresponding also to the E_1 and E_2 absorption bands in these garnets (Figure 7a). The difference in the position of these bands $\Delta E = E_2 - E_1$, proportional to the crystal field strength in the dodecahedral position of garnet, is equal to 0.872, 0.894, and 0.905 eV for samples 2, 3, and 4 of $Y_{3-x}Ca_xAl_{5-y}Si_yO_{12}$:Ce SCFs, respectively (see Figure 7). These ΔE values deviate somewhat from the values of $\Delta E = 0.93$ eV in YAG:Ce SCFs. Meanwhile, the Stokes shift, the difference in the position of emission and low-energy excitation bands, is much lower in sample 2 (66 nm; 0.342 eV) and sample 5 (81 nm; 0.41 eV) of $Y_{3-x}Ca_xAl_{5-y}Si_yO_{12}$:Ce SCFs compared to the YAG:Ce SCF (84.5 nm; 0.422 eV).
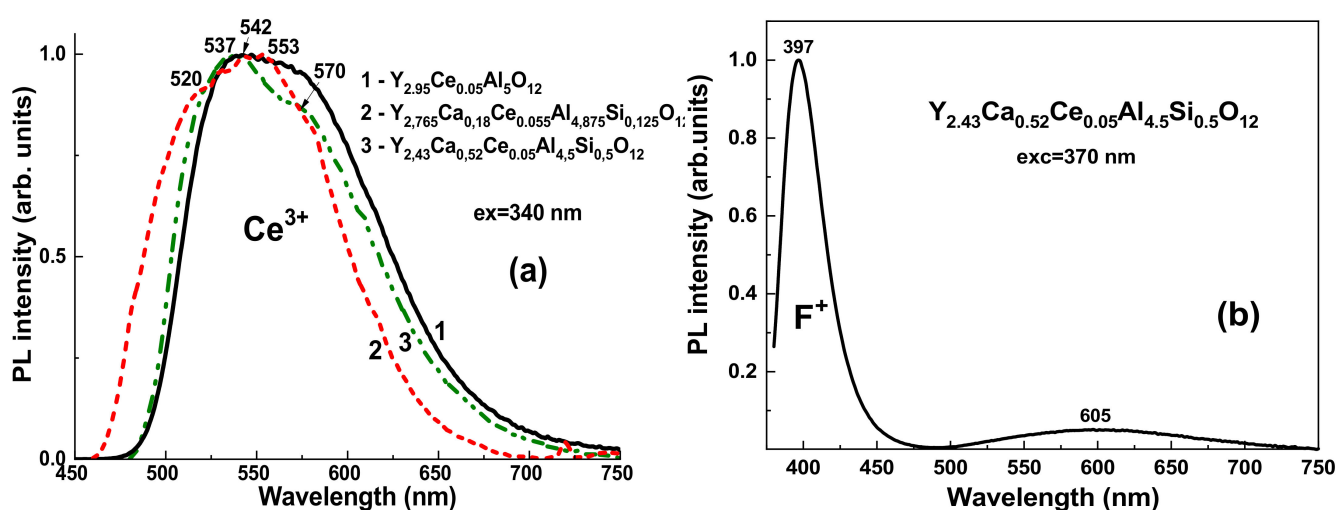
Figure 6. (**a**)—RT PL spectra of $Y_{3-x}Ca_xAl_{5-y}Si_yO_{12}$:Ce SCF with different Ca and Si content x/y = 0.18/0.125 (2) and y = 0.52/0.5 (3) in comparison with PL spectra of YAG:Ce SCF (1) under excitation in the vicinity of Ce^{3+} absorption band at 340 nm. (**b**)—RT PL spectra of F^+ center in $Y_{2.43}Ca_{0.52}Ce_{0.05}Al_{4.5}Si_{0.5}O_{12}$ SCF under excitation at 370 nm in the respective absorption band of this center.
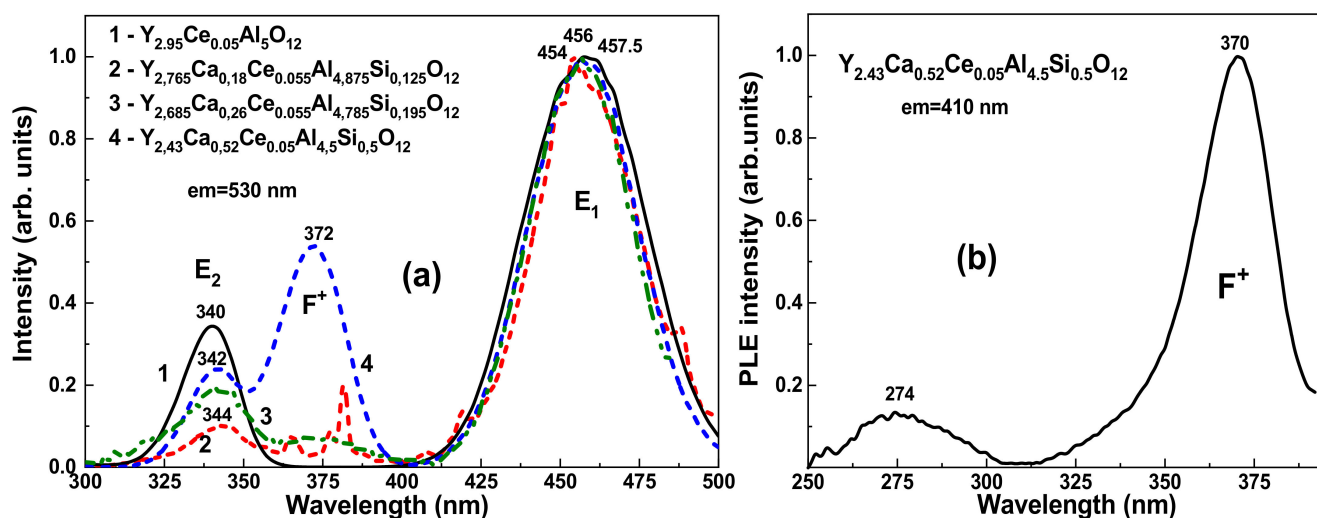
Figure 7. (**a**)—RT excitation spectra of Ce^{3+} luminescence at 530 nm in $Y_{3-x}Ca_xAl_{5-y}Si_yO_{12}$:Ce SCFs with different Ca and Si content (2–4) in comparison with respective excitation spectra in YAG:Ce SCF (1). (**b**)—RT excitation spectra of F^+ center luminescence in $Y_{2.43}Ca_{0.52}Ce_{0.05}Al_{4.5}Si_{0.5}O_{12}$ SCF at registration of emission at 400 nm.

The band peaking at 372 nm in the excitation spectra of the Ce^{3+} luminescence in $Y_{3-x}Ca_xAl_{5-y}Si_yO_{12}$:Ce SCFs at x values in the 0.26–0.52 range is connected to the intrinsic 1A→1B transitions of the F^+ center [30]. The association of this band with F^+ centers proves the availability of the characteristic excitation bands of these centers at 370 nm and 274 nm in the $Y_{2.43}Ca_{0.52}Ce_{0.05}Al_{4.5}Si_{0.5}O_{12}$ SCF at a registration of emission at 410 nm (Figure 7b). As a result, the Ce^{3+} centers in these SCFs can be excited by the luminescence of F^+ centers in the 397 nm band, which strikingly overlapped with the E_2 absorption bands of Ce^{3+} ions (Figure 4).

3.4. Decay Kinetics of Photoluminescence

In comparison to the YAG:Ce SCF counterpart, the decay kinetics of the Ce^{3+} luminescence in the $Y_{3-x}Ca_x Al_{5-y}Si_yO_{12}$:Ce SCFs with different Ca and Si content in the x = 0.13–0.52 and y = 0.065–0.5 ranges, respectively, under excitation at 340 nm in the vicinity of E_2 Ce^{3+} absorption bands are shown in Figure 8a. Similar to other Ca^{2+}-Si^{4+}-based garnets [13,24,31] and contrary to the YAG:Ce SCFs (Figure 8a, curves 1), the decay kinetics of the $Y_{3-x}Ca_xAl_{5-y}Si_yO_{12}$:Ce SCFs (Figure 8a, curves 2–5) are strongly nonexponential, and the decay curves become faster and nonexponential when increasing the x and y values. For this reason, these decay curves can be presented by the two or even more components with the characteristic decay time values **t** at 1/e: 0.1 and 0.001 intensity decay levels (Figure 8a). The respective decay times $\tau_{1/e}$, $\tau_{1/10}$, and $\tau_{1/100}$ are presented in Table 2.

The key reasons for the nonexponential decay kinetics of the Ce^{3+} luminescence in the as-grown $Y_{3-x}Ca_xAl_{5-y}Si_yO_{12}$:Ce SCFs are the presence of Ce^{4+} valence states and the formation of Ce1 and Ce2 multicenters due to the substitution of Ca^{2+} and Y^{3+} cations by Ce^{3+} ions, accordingly. The effect of the acceleration of the Ce^{3+} decay in the case of Ce^{4+} presence can also potentially be related to the direct intervalence charge transfer (IVCT) transitions that induce fast nonradiative decay channels [33–35]. This effect has recently been described for Eu^{2+}/Eu^{3+} pairs in fluorides by L. Seijo et al. [33] and also predicted for Ce^{3+}/Ce^{4+} pairs in SrS [34] and garnet compounds [35].
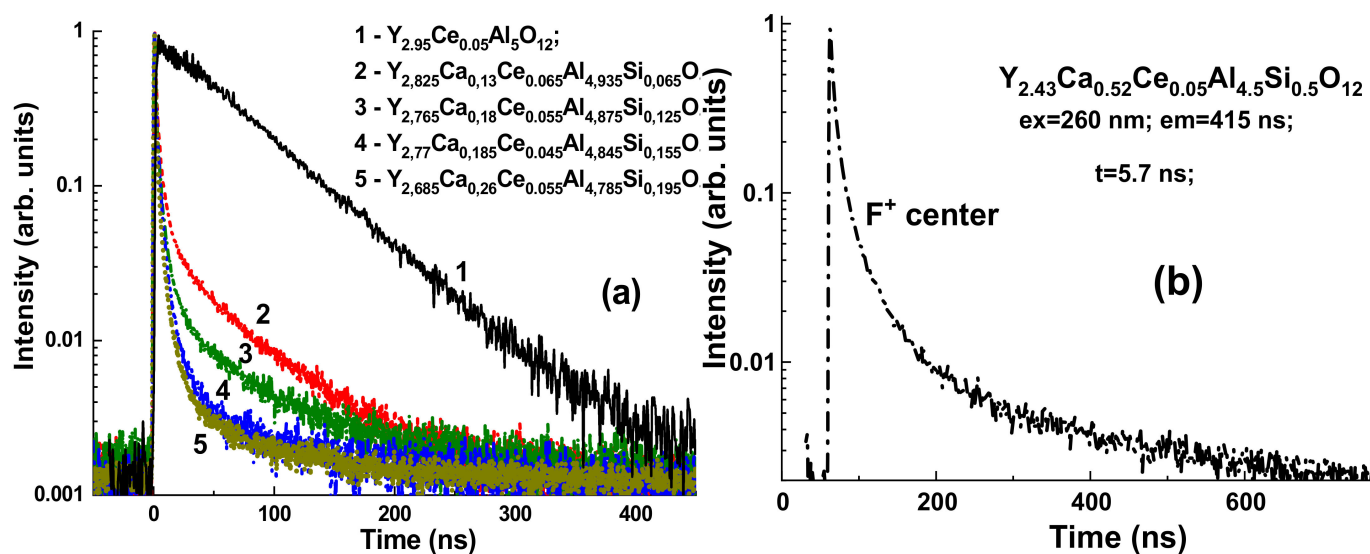
Figure 8. (**a**)—RT decay kinetics of Ce^{3+} luminescence at 530 nm in $Y_{3-x}Ca_xAl_{5-x}Si_yO_{12}$:Ce SCFs with different Ca and Si content (2–5) under excitation of PL at 340 nm and registration of PL at 530 nm in comparison with respective decay kinetics of Ce^{3+} emission in YAG:Ce SCFs (1). (**b**)—RT decay kinetics of F^+ luminescence at 415 nm in $Y_{2.43}Ca_{0.52}Ce_{0.05}Al_{4.5}Si_{0.5}O_{12}$ SCFs.

Table 2. Decay times of PL at RT in $Y_{3-x}Ca_xAl_{5-y}Si_yO_{12}$:Ce SCFs with different Ca and Si content under excitation at 340 nm and registration of PL at 530 nm.

No	Real SCF Content	$t_{1/e}$,ns	$t_{1/10}$,ns	$t_{1/100}$,ns
R	$Y_{2.95}Ce_{0.05}Al_5O_{12}$:Ce	62.6	141	294
1	$Y_{2.825}Ca_{0.13}Ce_{0.065}Al_{4.935}Si_{0.065}O_{12}$	2.9	8.5	86.2
2	$Y_{2.765}Ca_{0.18}Ce_{0.055}Al_{4.875}Si_{0.125}O_{12}$	2.95	6.6	39
3	$Y_{2.77}Ca_{0.185}Ce_{0.045}Al_{4.845}Si_{0.155}O_{12}$	2.0	5.7	21.8
4	$Y_{2.685}Ca_{0.26}Ce_{0.055}Al_{4.785}Si_{0.195}O_{12}$	1.95	4.8	18.2
5	$Y_{2.43}Ca_{0.52}Ce_{0.05}Al_{4.5}Si_{0.5}O_{12}$	1.6	7.5	29.5

The Ce^{4+} ions, which act as very effective electron trapping centers, can significantly accelerate the decay kinetics of Ce^{3+} luminescence when excited with energies higher than the band gap of garnet or close to the energies of the $O^{2-}{\rightarrow}Ce^{4+}$ CTT [36,37]. Due to the extended long-wavelength wings of these CTT bands in the garnets under study, the presence of $O^{2-}{\rightarrow}Ce^{4+}$ transitions is also feasible under 340 nm excitation in the area of the E_2 absorption band of Ce^{3+} ions [36,37]. Therefore, even under 340 nm excitation, we can observe the luminescence of Ce^{3+} ions due to the charge transformation of Ce^{4+} ions: $Ce^{4+} + hv_{(340\,nm)}{\rightarrow}(Ce^{3+})*+p{\rightarrow}Ce^{3+}_{(530\,nm)}+p{\rightarrow}Ce^{4+}$ [22,23].

Under this supposition, the Ce^{4+} centers can be responsible for the presence of the fast components of cerium luminescence with a lifetime of $t_{1/e}$ = 3.5–5.85 ns in $Y_{2.43}Ca_{0.52}Ce_{0.05}Al_{4.5}$ $Si_{0.5}O_{12}$ SCF when excited at 340 nm. In the meantime, the slower decay components of luminescence in these garnets, with decay times of $t_{1/20}$ = 49.4–62.9 ns and 98–121 ns, are mostly attributable to Ce^{3+} ion radiative transitions. The decay time constants of the Ce^{3+} luminescence in YAG:Ce SCF are $t_{1/e}$ = 60.5 ns and $t_{1/20}$ = 183 ns, correspondingly (Figure 8a, curve 1).

It is worth noting that the presence of the fast component of cerium luminescence in the ns range in silicate garnet compounds and the nonexponential form of the decay curves are also related to the formation of Ce^{3+} multicenters [13,14,21–25]. In particular, such decay curves can imply the possibility of energy transfer between low-energy and high-energy emitting Ce^{3+}-based centers [25]. Nonetheless, in the as-grown $Y_{3-x}Ca_xAl_{5-y}Si_yO_{12}$:Ce SCFs, the contribution of such an energy transfer mechanism to the nonexponential kinetics of PL is strongly masked by the presence of Ce^{4+} centers. Therefore, the study of the influence of the energy transfer processes between Ce^{3+} multicenters on the nonexponential kinetics of the Ce^{3+} luminescence in these garnets can be performed only after removing the Ce^{4+} centers, for instance, by using the thermal annealing of SCFs in the reducing atmosphere [33].

3.5. Scintillation Properties of Ce^{3+} Doped $Y_{3-x}Ca_xAl_{5-y}Si_yO_{12}$ SCFs

Under α-particle excitation by a ^{239}Pu (5.15 MeV) source, the as-grown $Y_{3-x}Ca_xAl_{5-y}$ Si_yO_{12}:Ce SCFs show significantly lower scintillation LY in comparison with the YAG: Ce SCF counterpart with an LY of 2.6 photons per keV (Table 3). The low scintillation efficiency of Ca-Si-based SCFs is due to the recharging of the majority of Ce^{3+} ions to the Ce^{4+} state in as-grown samples. The scintillation behavior of $Y_{3-x}Ca_xAl_{5-y}Si_yO_{12}$:Ce SCFs corresponds to the properties of $Ca_3ScSi_3O_{12}$:Ce and $Ca_2YMgScSi_3O_{12}$:Ce SCFs [23–25], as well as (Lu, Y)$_2SiO_5$: Ce SCFs [38,39], where the low scintillation response is caused by the main Ce^{4+} valence state of cerium ions, which formed during the LPE growth of these SCFs from the flux based on PbO oxide.

The scintillation decay kinetics of $Y_{3-x}Ca_xAl_{5-y}Si_yO_{12}$:Ce SCFs are presented in Figure 9. As can be seen from this figure, the scintillation response of these SCFs becomes faster with increasing the Ca-Si concentrations. The respective decay times are equal to $t_{1/e}$ = 50 ns, 43.5, and 30 ns and $t_{1/20}$ = 152 ns, 148 ns, and 79 ns for SCF samples with Ca/Si content x/y = 0.18/0.125, 0.26/0.195, and 0.52/0.5, respectively, in comparison with $t_{1/e}$ = 50 ns and $t_{1/20}$ = 152 ns for YAG: Ce SCF. This effect also correlates with the

significant decrease in the LY of $Y_{3-x}Ca_xAl_{5-y}Si_yO_{12}$:Ce SCF samples when increasing the Ca/Si concentration (Table 3).

Table 3. Scintillation LY and $t_{1/e}$, $t_{1/20}$ decay times of $Y_{3-x}Ca_xAl_{5-y}Si_yO_{12}$:Ce SCFs with different Ca and Si content under excitation by particles of ^{239}Pu (5.15 MeV) in comparison with YAG: Ce standard sample with an LY of 2.6 photons/keV. *—not measured.

No	SCF Content	LY, %	$t_{1/e}$, ns	$t_{1/e}$, ns
R	$Y_{2.95}Ce_{0.05}Al_5O_{12}$:Ce	100	141	294
1	$Y_{2.825}Ca_{0.13}Ce_{0.065}Al_{4.935}Si_{0.065}O_{12}$	9.5	8.5	86.2
2	$Y_{2.765}Ca_{0.18}Ce_{0.055}Al_{4.875}Si_{0.125}O_{12}$	8.5	6.6	39
3	$Y_{2.77}Ca_{0.185}Ce_{0.045}Al_{4.845}Si_{0.155}O_{12}$	7.0	5.7	21.8
4	$Y_{2.685}Ca_{0.26}Ce_{0.055}Al_{4.785}Si_{0.195}O_{12}$	6.6	4.8	18.2
5	$Y_{2.43}Ca_{0.52}Ce_{0.05}Al_{4.5}Si_{0.5}O_{12}$	5.9	7.5	29.5
5a	$Y_{2.43}Ca_{0.52}Ce_{0.05}Al_{4.5}Si_{0.5}O_{12}$; TT = 1000 °C	10.9	*	*
5b	$Y_{2.43}Ca_{0.52}Ce_{0.05}Al_{4.5}Si_{0.5}O_{12}$; TT = 1300 °C	38	44.3	152

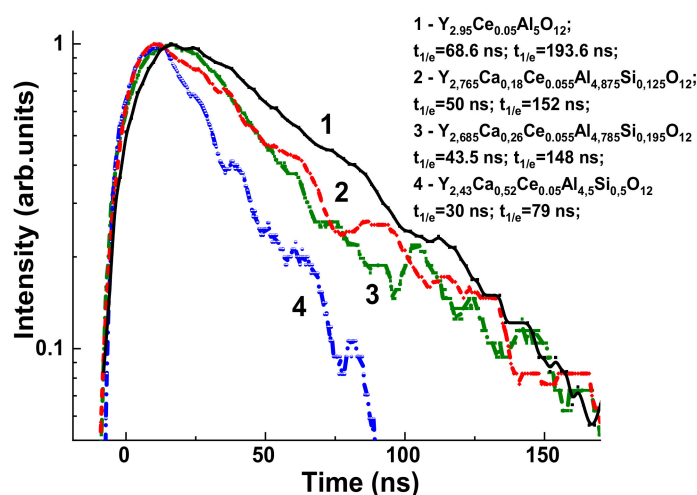**Figure 9.** Scintillation decay kinetics of $Y_{3-x}Ca_xAl_{5-y}Si_yO_{12}$:Ce SCFs with different Ca and Si content under excitation by α–particles of ^{239}Pu (5.15 MeV) source in comparison with respective scintillation decay kinetics of YAG: Ce SCF (1).

4. Optical Properties of $Y_{3-x}Ca_xAl_{5-y}Si_yO_{12}$ SCFs, Annealing in the Reducing Atmosphere

The impact of thermal treatment (TT) at the 1000–1300 °C range in the 95% N_2–5% H_2 reducing atmosphere on the optical properties of $Y_{3-x}Ca_xAl_{5-y}Si_yO_{12}$:Ce SCFs was investigated as well (Figures 10–12) with the example of the $Y_{2.43}Ca_{0.52}Ce_{0.05}Al_{4.5}Si_{0.5}O_{12}$ SCF sample. The mentioned TT results in the change of the relative concentration of Ce^{4+} and Ce^{3+} centers in the SCFs under study due to the reaction $O^{2-} + 2Ce^{4+} \rightarrow V_O + 2Ce^{3+}$, where V_O is the oxygen vacancy.

The different absorption spectra of the untreated and annealed samples at 1000 °C and 1300 °C support this result (Figure 10, curves 4 and 5, respectively).

As shown in Figure 10, the intensity of the $O^{2-} \rightarrow Ce^{4+}$ CTT absorption band in the UV region, peaking at 250 nm, falls significantly in annealed samples. This decrease in absorption of Ce^{4+} centers is accompanied by an increase in absorption in the bands peaking at 446 and about 340 nm, which correspond to the E_1 and E_2 absorption bands of Ce^{3+} ions. Additionally, the rate of increase in the Ce^{3+} absorption is proportionate to the annealing temperature (Figure 10, curves 4 and 5).
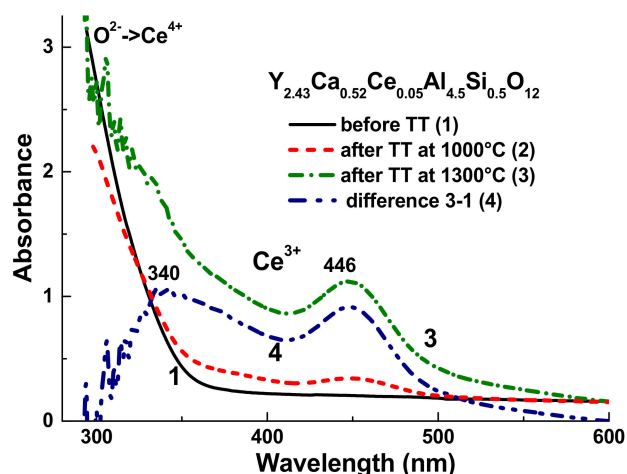
Figure 10. Influence of the TT in N_2 95% + H_2 5% atmosphere at 1000 °C (2) and 1300 °C (3) temperatures on the absorption spectra of $Y_{2.43}Ca_{0.52}Ce_{0.05}Al_{4.5}Si_{0.5}O_{12}$ SCF. Curve 4 is the difference spectra of untreated and annealed samples at temperature of 1300 °C.

The annealing of $Y_{2.43}Ca_{0.52}Ce_{0.05}Al_{4.5}Si_{0.5}O_{12}$ SCF in a reducing environment causes a significant change in the structure emission and excitation bands, which is connected with Ce^{3+} centers. Particularly, in the as-grown sample, the maximum of the Ce^{3+} emission band is located at 540 nm in the as-grown sample, excited in the major bands peaking at 458 nm, and bumped at 342 nm (Figure 11, curve 1). We assumed that these bands are linked to the Ce1 center. The difference in the locations of the E_1 and E_2 excitation bands for such a Ce1 center is 0.917 eV. For this center, the difference in the locations of the emission and low-energy excitation bands (Stokes shift) is 82 nm (0.41 eV).

The excitation band peaking at the 380–385 nm range is related to the excitation of F^+ center emission and follows the excitation of the Ce^{3+} luminescence via the emission of these centers.
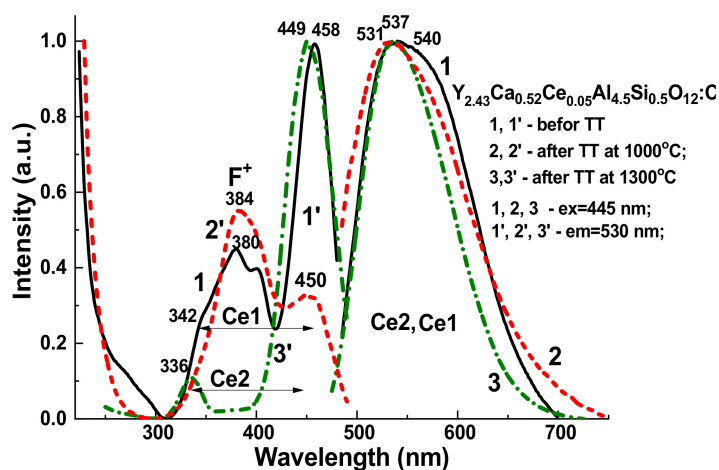

Figure 11. Influence of the thermal treatment in N_2 95% + H_2 5% atmosphere at 1000 °C (2) and 1300 °C (3) temperatures on the excitation spectra (1–3) and emission spectra (1′–3′) of Ce^{3+} luminescence in $Y_{2.43}Ca_{0.52}Ce_{0.05}Al_{4.5}Si_{0.5}O_{12}$ SCF sample.

Meanwhile, the TT at a temperature of 1000 °C and 1300 °C results in: (i) a significant shift in the maximum of the Ce^{3+} emission spectrum to 531 and 537 nm; (ii) a shift of the main excitation bands to 450 and 449 nm, respectively; and (iii) a strong decrease of the intensity of the F^+ center excitation band peaking at 380 nm and the appearance of an excitation band peaking at 336 nm. After TT, such changes in the emission and excitation spectra of $Y_{2.43}Ca_{0.52}Ce_{0.05}Al_{4.5}Si_{0.5}O_{12}$ SCFs can be attributed to an increase in the relative

concentrations of Ce2 centers. For such a Ce2 center, the difference in the positions of E_1 and E_2 excitation bands is equal to 0.928 eV. Therefore, the Ce2 centers are characterized by a slightly larger crystal field strength than that of the Ce1 centers, and for this reason, the position of emission bands of this center is redshifted with respect to the Ce1 center. The Stokes shift of the Ce2 center is equal to 88 nm (0.452 eV).

Figure 12a displays the effect of the TT in the N_2 95% + H_2 5% atmosphere at temperatures of 1000 °C and 1300 °C on the decay kinetics of the Ce^{3+} luminescence in $Y_{2.43}Ca_{0.52}Ce_{0.05}Al_{4.5}Si_{0.5}O_{12}$ SCF. Annealing in a reducing environment reduces the concentration of Ce^{4+} centers while increasing the content of Ce^{3+} centers, resulting in variations in the decay kinetics of the SCF samples. Particularly, the treatment in the 1000–1300 °C range provides more flat-shaped decay curves of the Ce^{3+} luminescence. This suggests that the intrinsic transitions of Ce^{3+} ions have a dominant contribution to the PL decay kinetics of $Y_{2.43}Ca_{0.52}Ce_{0.05}Al_{4.5}Si_{0.5}O_{12}$ SCF after TT, specifically in the sample annealed at 1300 °C (Figure 12, curve 3). Taking into account the dominant contribution of the Ce2 centers to the PL of this sample, the decay kinetics of SCFs, annealed at 1300 °C, are mostly connected to the luminescence of this center. The $Ce^{4+} \rightarrow Ce^{3+}$ recharge in SCF samples after TT allows investigating the possibility of energy transfer across various Ce^{3+} multicenters in the $Y_{2.43}Ca_{0.52}Ce_{0.05}Al_{4.5}Si_{0.5}O_{12}$ garnet. Specifically, the slightly nonexponential form of Ce^{3+} luminescence in the SCF sample treated at 1300 °C (Figure 12a, curve 3) can be generated by energy transfer between Ce1 and Ce2 centers.
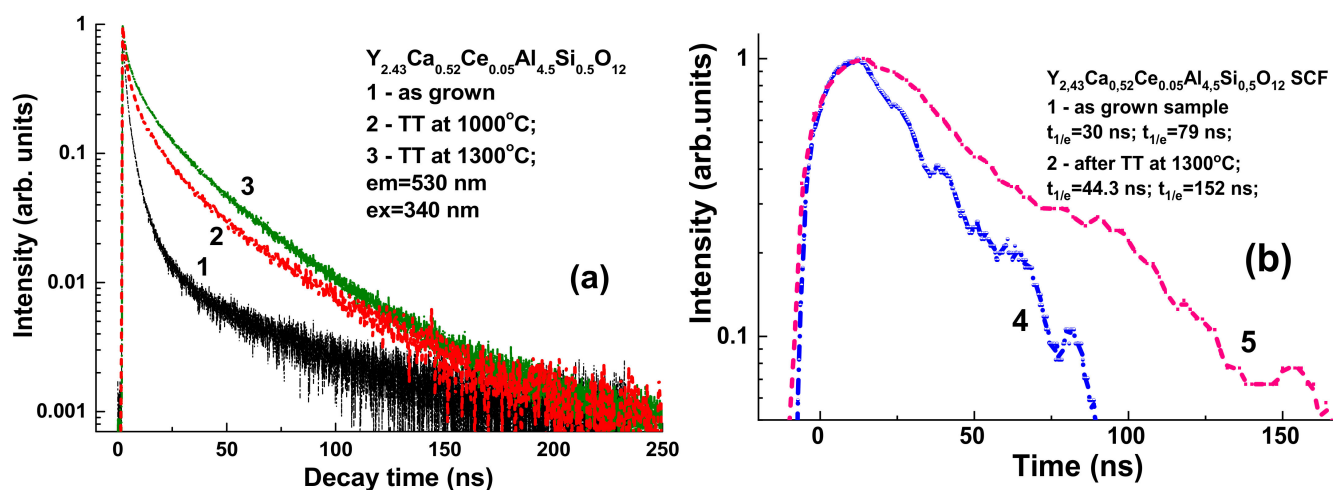

Figure 12. (**a**)—RT decay kinetics of Ce^{3+} luminescence at 530 nm in $Y_{2.43}Ca_{0.52}Ce_{0.05}Al_{4.5}Si_{0.5}O_{12}$ SCFs under excitation of PL at 340 nm and registration of PL at 530 nm before (1) and after TT in the reducing N_2 + H_2 (95 + 5%) atmosphere at 1000 °C (2) and 1300 °C (3). (**b**)—Scintillation decay kinetics of this SCF after TT at 1300 °C (2) in comparison with as-grown sample (1).

The abovementioned conclusion is confirmed by the measurements of the scintillation LY of the $Y_{2.43}Ca_{0.52}Ce_{0.05}Al_{4.5}Si_{0.5}O_{12}$ SCF after TT at 1000 °C and 1300 °C in the reducing (N_2 + H_2) atmosphere. Specifically, a significant (up to 1.4 times) rise in LY is seen after TT of this sample even at 1000 °C due to the recharging of certain part of Ce^{4+} ions to the Ce^{3+} form (Table 2). Simultaneously, the TT of the SCF at 1300 °C resulted in a greater (up to 6.5 times) increase in LY when compared to the untreated sample. Furthermore, the scintillation decay kinetics of this SCF sample also become slower and close to YAG:Ce SCF (Figure 12b) due to the recharging of the significant part of the Ce^{4+} ions to the Ce^{3+} state. However, the significant part of the LY in the annealed sample is probably lost due to the formation of the large concentration of oxygen vacancies and the strong continuous absorption of this sample in the range of the Ce^{3+} luminescence (see Figure 10, curve 5).

5. Regularities of $Ce^{3+} \leftrightarrow Ce^{4+}$ Recharge in $Y_{3-x}Ca_xAl_{5-y}Si_yO_{12}$:Ce SCFs

The comparison of the absorption spectra of $Y_{3-x}Ca_xAl_{5-y}Si_yO_{12}$:Ce and YAG:Ce SCFs (Figure 3) as well as the absorption spectra of the initial and annealed in the reducing atmosphere of $Y_{2.43}Ca_{0.52}Ce_{0.05}Al_{4.5}Si_{0.5}O_{12}$ SCF sample (Figure 10) clearly confirms *the formation of the main part of cerium ions in the Ce^{4+} state for the compensation of the access of Ca^{2+} ions in the as-grown SCFs of these garnets*. Meanwhile, in contradiction with the dominant Ce^{4+} state in the as-grown SCFs, the CL spectra, and the scintillation decay kinetics of these samples confirm that the energy transfer from garnet host to the emission centers is realized in the final stage via *the Ce^{3+} luminescence*. This means that the excitation of the Ce^{3+} center emission in the $Y_{3-x}Ca_xAl_{5-y}Si_yO_{12}$:Ce SCFs under high energy irradiation (e-beam, α-particles) occurs via the initial recharging of Ce^{4+} ions instead of the direct excitation of the Ce^{3+} luminescence in the YAG:Ce SCF counterpart.

The excitation processes of the Ce^{3+} luminescence in the $Y_{3-x}Ca_xAl_{5-y}Si_yO_{12}$:Ce SCFs with preferable Ce^{4+} state under high-energy excitation can be presented as follows (Figure 13) [40–42]. At the initial stage of the CL/scintillation process, the ionizing radiation produces electron-hole pairs. The trapping of electrons from the conductive band by the Ce^{4+} ions leads to the formation of Ce^{3+} centers in the excited state (step1). Their radiative decay results in the appearance of the Ce^{3+} emission and formation of the temporary Ce^{3+} ions in the ground state (step 2), which trap mobile holes from the valence band (step 3), and, as a consequence, Ce^{4+} centers are recreated.
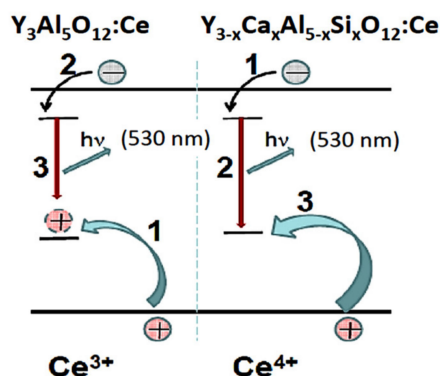

Figure 13. The difference in the mechanism of excitation of Ce^{3+} and Ce^{4+} luminescence in YAG: Ce and $Y_{3-x}Ca_xAl_{5-y}Si_yO_{12}$:Ce SCFs.

The preferable excitation of the Ce^{3+} luminescence via the recharging of Ce^{4+} ions in $Y_{3-x}Ca_xAl_{5-y}Si_yO_{12}$:Ce SCFs can result also in the strong acceleration of their scintillation decay kinetics (Figure 9). Indeed, the processes of the excitation of the Ce^{3+} luminescence in these SCFs can decrease the delay in the migration stage of the energy transfer from the excited garnet hosts to the Ce^{3+} ions due to the exclusion of the trapping of the charge carriers at the matrix defects [41,42] and unwanted impurities (e.g., Pb^{2+} flux related dopant). Such slowing of energy transfer is typically realized under high-energy excitation in the Ce^{3+}-doped SCFs grown from PbO-B_2O_3 based fluxes [43].

The respective changes in the absorption and PL emission/excitation spectra and decay kinetics in the $Y_{2.43}Ca_{0.52}Ce_{0.05}Al_{4.5}Si_{0.5}O_{12}$ SCFs were observed. They are related to the change in concentration of the Ce^{4+} and Ce^{3+} centers after TT in the 1000–1300 °C range, and they confirm the assumption regarding the formation of Ce^{3+} multicenters in $Y_{3-x}Ca_xAl_{5-y}Si_yO_{12}$:Ce Ce SCFs and the nature of Ce1 and Ce2 centers in these garnets. The Ce1 centers are formed by Ce^{3+} ions at the Y^{3+} sites, whereas Ce2 centers form when Ce^{3+} ions replace the Ca^{2+} cations. However, due to the main Ce^{4+} valence state of Ce2 centers in as-grown samples, these centers are barely visible in the PL emission and excitation spectra, as well as the decay kinetics of the Ce^{3+} luminescence (Figures 6–8). Ad interim, treatment in the reducing environment causes a part of the Ce^{4+} ions to be

recharged to the Ce^{3+} states, allowing the detection of the Ce2 centers in the PL spectra and the PL decay kinetics of the Ce^{3+} emission (Figures 10 and 11).

6. Conclusions

The growth of the single crystalline films (SCFs) of $Y_{3-x}Ca_xAl_{5-y}Si_yO_{12}$:Ce garnets at Ca and Si concentration in the x = 0.13–0.52 and y = 0.065–0.5 ranges, respectively, was performed using the LPE method from $PbO-B_2O_3$ based flux onto $Y_3Al_5O_{12}$ (YAG) substrates. Due to Ca^{2+} and Si^{4+} alloying in the mentioned compounds, the misfit between SCF-substrate lattice constants changed from 0 to 0.53%. The segregation coefficients of Ca and Si ions in the SCFs under study are nonlinearly changed in the 0.17–0.28 and y = 0.065–0.25 ranges, respectively, when changing the nominal Ca and Si content in the melt solution in the x = 0.5–2 range. The segregation coefficient of Ce^{3+} ions in the $Y_{3-x}Ca_xAl_{5-y}Si_yO_{12}$:Ce SCFs was equal to 0.007–0.0095.

We have also found that the real Ca and Si content in $Y_{3-x}Ca_xAl_{5-y}Si_yO_{12}$:Ce SCFs is not equal at the equimolar concentration of these ions in the melt solution: the Ca^{2+} content was systematically larger than that of the Si^{4+}. Both types of charge compensation of the Ca^{2+} excess are expected in these SCFs: the predominant formation of Ce^{4+} and Pb^{4+} states at relatively low Ca-Si content and the preferable formation of oxygen vacancies at a large Ca-Si concentration.

The absorption, luminescent, and scintillation properties of $Y_{3-x}Ca_xAl_{5-y}Si_yO_{12}$:Ce SCFs were investigated and compared with those for the reference YAG:Ce SCF counterpart. The cathodoluminescence spectra of Ce^{3+} ions in $Y_{3-x}Ca_xAl_{5-y}Si_yO_{12}$:Ce SCFs are significantly extended in the red range compared to YAG:Ce SCF due to the formation of Ce^{3+} multicenters in the dodecahedral positions of the garnet lattices, additionally stimulated by the Ca^{2+} and Si^{4+} pair co-doping.

We have confirmed the formation of two types of Ce^{3+} centers in the $Y_{3-x}Ca_xAl_{5-y}Si_yO_{12}$:Ce garnets in the photoluminescence emission and excitation spectra SCFs of these compounds. These two centers (Ce1 and Ce2) possess various local surroundings due to the substitution by the Ce^{3+} ions of different dodecahedral cation positions (correspondingly Y^{3+} and Ca^{2+}) and are characterized by differing spectral behaviors.

The fast F^+ center luminescence band peaking at 372 nm and with a decay time of 5.7 ns is observed in $Y_{3-x}Ca_xAl_{5-y}Si_yO_{12}$:Ce SCFs at Ca (x) and Si (y) content approximately above 0.2. Due to the overlapping of the emission band of F^+ centers with the absorption band of Ce^{3+} ions, Ce^{3+} luminescence in these SCFs can be partly excited via emission of F^+ centers.

The as-grown $Y_{3-x}Ca_xAl_{5-y}Si_yO_{12}$:Ce SCFs show poor scintillation properties. Under α–particles excitation by ^{239}Pu (5.15 MeV) source, these SCFs possess a faster scintillation response with decay times in the $t_{1/e}$ = 50–30 ns and $t_{1/20}$ = 152–70 ns ranges but significantly low light yield (LY) of 6–8% in comparison with the reference YAG:Ce SCF (LY = 100%; $t_{1/e}$ = 66 ns; $t_{1/20}$ = 194 ns). At the same time, the LY of as-grown $Y_{3-x}Ca_xAl_{5-y}Si_yO_{12}$:Ce SCFs can significantly increase (up to 1.4–6.5 times) after their thermal treatment (TT) in the reducing atmosphere (95% N_2 + 5% H_2) at temperatures in the range of 1000–1300 °C.

We have also observed the formation of Ce^{4+} valence states in the optical properties of $Y_{3-x}Ca_xAl_{5-y}Si_yO_{12}$:Ce SCFs. The presence of Ce^{4+} ions in the as-grown SCFs is confirmed by the observation of the $O^{2+}-Ce^{4+}$ charge transfer transitions in the absorption spectra of these SCFs. The Ce^{4+} centers are also responsible for acceleration of the initial stage of the PL decay kinetics of cerium and the presence of fast components with a lifetime in the few ns range in these SCFs. The $Ce^{4+} \rightarrow Ce^{3+}$ recharge in these SCFs is achieved by the TT in the reducing atmosphere at temperatures above 1000 °C. Such TT also leads to more exponential-like decay kinetics of the Ce^{3+} luminescence in $Y_{3-x}Ca_xAl_{5-y}Si_yO_{12}$:Ce SCFs and enables studying the energy transfer processes between the different Ce^{3+} multicenters in these garnets.

Author Contributions: V.G. performed SCF growth experiments and participated in writing the growth part of the paper; T.Z. performed the absorption and scintillation measurements; A.S. perform the annealing of samples; S.W.-Ł. performed the cathodoluminescence and content measurements, analyzed the results in whole, and contributed to the paper preparation; A.F. measured the XRD patterns of the SCF samples; A.O. performed the photoluminescence decay measurements; M.B. participated in the writing and preparation of the paper; and Y.Z. analyzed all the experimental materials and wrote the main part of the paper. All authors have read and agreed to the published version of the manuscript.

Conflicts of Interest: The authors declare no conflict of interest.

References

1. Bardsley, N.; Bland, S.; Pattison, L.; Pattison, M.; Stober, K.; Welsh, F.; Yamada, M. *Solid-State Lighting R&D. Multi-Year Program Plan*; US Energy Depart: Washington, DC, USA, 2014.
2. Ching, S.; Chang, Y.; Yang, T.; Chung, T.; Chen, C.; Lee, T.; Li, D.; Lu, C.; Ting, Z.; Glorieux, B.; et al. Packaging efficiency in phosphor-converted white LEDs and its impact to the limit of luminous efficacy. *J. Sol. State Light* **2014**, *1*, 19.
3. Raukas, M.; Kelso, J.; Zheng, Y.; Bergenek, K.; Eisert, D.; Linkov, A.; Jermann, F. Ceramic phosphors for light conversion in LEDs. *J. Solid State Sci. Technol.* **2013**, *2*, R3168–R3176. [CrossRef]
4. Rossner, W.; Wessler, B. Light Source Having an LED and a Luminescence Conversion Body and Method for Producing the Luminescence Conversion Body. U.S. Patent 7554258B2, 30 June 2009.
5. De Graaf, J.; Kop, T.A. Phosphor in Polycrystalline Ceramic Structure and a Light-emitting Element Comprising Same. U.S. Patent 7879258B2, 1 February 2011.
6. Miyagawa, H.; Nakamura, T.; Fujii, H.; Mochizuki, A. Method of Fabricating Translucent Phosphor Ceramics. U.S. Patent 8123981B2, 28 February 2012.
7. Miyagawa, H.; Nakamura, T.; Fujii, H.; Mochizuki, A. Method of Manufacturing Phosphor Translucent Ceramics and Light Emitting Devices. U.S. Patent 8137587B2, 20 March 2012.
8. Miyagawa, H.; Nakamura, T.; Fujii, H.; Mochizuki, A. Method of Manufacturing Phosphor Translucent Ceramics and Light Emitting Devices. U.S. Patent 8298442B2, 30 October 2012.
9. Nakamura, T.; Fujii, H.; Miyagawa, H.; Mukherjee, R.; Zhang, B.; Mochizuki, A. Luminescent Ceramic and Light-Emitting Device Using the Same. U.S. Patent 8339025B2, 25 December 2012.
10. De Graaf, J.; Kop, T.A. Phosphor in Polycrystalline Ceramic Structure and a Light-emitting Element Comprising Same. U.S. Patent 8496852B2, 30 July 2013.
11. Ooyabu, Y.; Nakamura, T.; Fujii, H.; Ito, H. Phosphor Ceramic and Light-Emitting Device. U.S. Patent 8664678B2, 5 January 2012.
12. Boerkekamp, J.G.; Steigelmann, O.; van Hal, H.A.M.; Cillessen, J.F.M. Light Scattering by Controlled Porosity in Optical Ceramics for LEDs. U.S. Patent 8728835B2, 20 May 2014.
13. Setlur, A.A.; Heward, W.J.; Gao, Y.; Srivastava, A.M.; Chandran, R.G.; Shankar, M.V. Crystal Chemistry and Luminescence of Ce^{3+}-Doped $Lu_2CaMg_2(Si,Ge)_3O_{12}$ and Its Use in LED Based Lighting. *Chem. Mater.* **2006**, *18*, 3314. [CrossRef]
14. Shimomura, Y.; Honma, T.; Shigeiwa, M.; Akai, T.; Okamoto, K.; Kijima, N. Sensors and Displays: Principles, Materials, and Processing—Photoluminescence and Crystal Structure of Green-Emitting $Ca_3Sc_2Si_3O_{12}$: Ce^{3+} Phosphor for White Light Emitting Diodes. *J. Electrochem. Soc.* **2007**, *154*, J35–J38. [CrossRef]
15. Katelnikovas, A.; Bettentrup, H.; Uhlich, D.; Sakirzanovas, S.; Jüstel, T.; Kareiva, A. Synthesis and optical properties of Ce^{3+}-doped $Y_3Mg_2AlSi_2O_{12}$ phosphors. *J. Lumin.* **2009**, *129*, 1356. [CrossRef]
16. Kishore, M.S.; Kumar, N.P.; Chandran, R.G.; Setlur, A.A. Solid Solution Formation and Ce^{3+} Luminescence in Silicate Garnets. *Electrochem. Solid-State Lett.* **2010**, *13*, J77. [CrossRef]
17. Zhong, J.; Zhuang, W.; Xing, X.; Liu, R.; Li, Y.; Liu, Y.; Hu, Y. Synthesis, Crystal Structures, and Photoluminescence Properties of Ce^{3+}-Doped $Ca_2LaZr_2Ga_3O_{12}$: New Garnet Green-Emitting Phosphors for White LEDs. *J. Phys. Chem. C* **2015**, *119*, 5562. [CrossRef]
18. Pan, Z.; Xu, Y.; Hu, Q.; Li, W.; Zhou, H.; Zheng, Y. Combination cation substitution tuning of yellow-orange emitting phosphor $Mg_2Y_2Al_2Si_2O_{12}$:Ce^{3+}. *RSC Adv.* **2015**, *5*, 9489. [CrossRef]
19. Li, G.; Tian, Y.; Zhao, Y.; Lin, J. Recent progress in luminescence tuning of Ce^{3+} and Eu^{2+}-activated phosphors for pc-WLEDs. *Chem. Soc. Rev.* **2015**, *44*, 8688. [CrossRef]
20. Shang, M.; Fan, J.; Lian, H.; Zhang, Y.; Geng, D.; Lin, J. A double substitution of Mg^{2+}–Si^{4+}/Ge^{4+} for Al $(1)^{3+}$–Al $(2)^{3+}$ in Ce^{3+}-doped garnet phosphor for white LEDs. *Inorg. Chem.* **2014**, *53*, 7748. [CrossRef]

21. Khaidukov, N.; Zorenko, T.; Iskaliyeva, A.; Paprocki, K.; Batentschuk, M.; Osvet, A.; van Deun, R.; Zhydachevskii, Y.; Zorenko, Y. Synthesis and luminescent properties of prospective Ce^{3+} doped silicate garnet phosphors for white LED converters. *J. Lumin.* **2017**, *192*, 328. [CrossRef]
22. Khaidukov, N.; Zorenko, Y.; Zorenko, T.; Iskaliyeva, A.; Paprocki, K.; Zhydachevskii, Y.; van Deun, R.; Batentschuk, M. New Ce^{3+} doped $Ca_2YMgScSi_3O_{12}$ garnet ceramic phosphor for white LED converters. *Phys. Status Solidi (RRL)* **2017**, *11*, 170001. [CrossRef]
23. Gorbenko, V.; Zorenko, T.; Paprocki, K.; Iskaliyeva, A.; Fedorov, A.; Schröppel, F.; Levchuk, I.; Osvet, A.; Batentschuk, M.; Zorenko, Y. Epitaxial growth of single crystalline film phosphors based on the Ce^{3+}-doped $Ca_2YMgScSi_3O_{12}$ garnet. *Cryst. Eng. Comm.* **2017**, *19*, 3689. [CrossRef]
24. Gorbenko, V.; Zorenko, T.; Pawlowski, P.; Iskaliyeva, A.; Paprocki, K.; Suchocki, A.; Zhydachevskii, Y.; Fedorov, A.; Khaidukov, N.; van Deun, R.; et al. Luminescent and scintillation properties of Ce^{3+} doped $Ca_2RMgScSi_3O_{12}$ (R = Y, Lu) single crystalline films. *J. Lumin.* **2018**, *195*, 362. [CrossRef]
25. Gorbenko, V.; Zorenko, T.; Witkiewicz, S.; Paprocki, K.; Iskaliyeva, A.; Kaczmarek, A.M.; van Deun, R.; Khaidukov, M.N.; Batentschuk, M.; Zorenko, Y. Luminescence of Ce^{3+} multicenters in Ca^{2+}-Mg^{2+}-Si^{4+} based garnet phosphors. *J. Lumin.* **2018**, *199*, 245–250. [CrossRef]
26. Ivanovskikh, K.; Meijerink, A.; Piccinelli, F.; Speghini, A.; Zinin, E.; Ronda, C.; Bettinelli, M. Optical spectroscopy of $Ca_3Sc_2Si_3O_{12}$, $Ca_3Y_2Si_3O_{12}$ and $Ca_3Lu_2Si_3O_{12}$ doped with Pr^{3+}. *J. Lumin.* **2010**, *130*, 893. [CrossRef]
27. Zhou, L.; Zhou, W.; Pan, F.; Shi, R.; Huang, L.; Liang, H.; Tanner, P.; Du, X.; Huang, Y.; Tao, Y.; et al. Spectral properties and energy transfer of a potential solar energy converter. *Chem. Mater.* **2016**, *28*, 2834. [CrossRef]
28. Zorenko, Y.; Gorbenko, V.; Voznyak, T.; Zorenko, T. Luminescence of Pb^{2+} ions in YAG:Pb single-crystalline films. *Phys. Stat. Sol.* **2008**, *245*, 1618. [CrossRef]
29. Scott, G.B.; Page, J.L. Pb valence in iron garnets. *J. Appl. Phys.* **1977**, *48*, 1342–1349. [CrossRef]
30. Zorenko, Y.; Zorenko, T.; Voznyak, T.; Mandowski, A.; Xia, Q.; Batentschuk, M.; Fridrich, J. Luminescence of F^+ and F centers in Al_2O_3-Y_2O_3 oxide compounds. *IOP Conf. Ser. Mater. Sci. Eng.* **2010**, *15*, 2060. [CrossRef]
31. Zorenko, Y.; Pashkovskii, M.; Limarenko, L.; Nazar, I.V. Antisite Defects in Fluorescence of Crystallophosphors with Garnet Structure. *Opt. Spektrosk.* **1996**, *80*, 698.
32. Zorenko, T.; Gorbenko, V.; Petrosyan, A.; Gieszczyk, W.; Bilski, P.; Zorenko, Y. Intrinsic and defect-related luminescence of $YAlO_3$ and $LuAlO_3$ single crystals and films. *Opt. Mater.* **2018**, *86*, 376. [CrossRef]
33. Barandiarán, Z.; Meijerink, A.; Seijo, L. Configuration coordinate energy level diagrams of intervalence and metal-to-metal charge transfer states of dopant pairs in solids. *Phys. Chem. Chem. Phys.* **2015**, *17*, 19874. [CrossRef] [PubMed]
34. Kulesza, D.; Cybińska, J.; Seijo, L.; Barandiarán, Z.; Zych, E. Anomalous red and infrared luminescence of Ce3+ ions in SrS: Ce sintered ceramics. *Phys. Chem. C.* **2015**, *119*, 27649. [CrossRef]
35. Phung, Q.M.; Barandiarán, Z.; Seijo, L. Structural relaxation effects on the lowest 4f–5d transition of Ce3+ in garnets. In *Proceedings of the 9th Congress on Electronic Structure: Principles and Applications (ESPA 2014)*; Springer: Berlin/Heidelberg, Germany, 2016; Available online: https://doi.org/10.1007/978-3-662-49221-5_15 (accessed on 23 May 2021).
36. Wu, Y.; Meng, F.; Li, Q.; Koschan, M.; Melcher, C.L. Role of Ce^{4+} in the Scintillation Mechanism of Codoped $Gd_3Ga_3Al_2O_{12}$:Ce. *Phys. Rev. Appl.* **2014**, *2*, 044009. [CrossRef]
37. Tyagi, M.; Meng, F.; Koschan, M.; Donnald, S.B.; Rothfuss, H.; Melcher, C.L. Effect of codoping on scintillation and optical properties of a Ce-doped $Gd_3Ga_3Al_2O_{12}$ scintillator. *J. Phys. D Appl. Phys.* **2013**, *46*, 475302. [CrossRef]
38. Zorenko, Y.; Gorbenko, V.; Savchyn, V.; Zorenko, T.; Grinyov, B.; Sidletskiy, O.; Fedorov, A. Growth and luminescent properties of Ce and Ce–Tb doped $(Y,Lu,Gd)_2SiO_5$:Ce single crystalline films. *J. Cryst. Growth* **2014**, *401*, 577. [CrossRef]
39. Zorenko, Y.; Gorbenko, V.; Bilski, P.; Twardak, A.; Mandowska, E.; Mandowski, A.; Sidletskiy, O. Comparative analysis of the scintillation and thermoluminescent properties of Ce-doped LSO and YSO crystals and films. *Opt. Mater.* **2014**, *369*, 1715. [CrossRef]
40. Dantelle, G.; Boulon, G.; Guyot, Y.; Testemale, D.; Guzik, M.; Kurosawa, S.; Kamada, K.; Yoshikawa, A. Research on Efficient Fast Scintillators: Evidence and X-Ray Absorption Near Edge Spectroscopy Characterization of Ce^{4+} in Ce^{3+} in Mg^{2+} -Co-Doped $Gd_3Al_2Ga_3O_{12}$ Garnet Crystal. *Phys. Status Solidi (B)* **2020**, *257*, 1900510. [CrossRef]
41. Chewpraditkul, W.; Warnak, C.; Szczesniak, T.; Moszcynski, M.; Jari, V.; Beitlerova, A.; Nikl, M. Comparison of absorption, luminescence and scintillation characteristics in $Lu_{1.95}Y_{0.05}SiO_5$:Ce,Ca and Y_2SiO_5:Ce scintillators. *Opt. Mater.* **2013**, *35*, 1679. [CrossRef]
42. Liu, S.; Feng, X.; Zhou, Z.; Nikl, M.; Shi, Y.; Pan, Y. Effect of Mg^{2+} co-doping on the scintillation performance of LuAG:Ce ceramics. *Phys. Status Solidi RRL* **2014**, *8*, 105. [CrossRef]
43. Zorenko, Y.; Gorbenko, V.; Zorenko, T.; Sidletskiy, O.; Fedorov, A.; Bilski, P.; Twardak, A. High-performance Ce-doped multicomponent garnet single crystalline film scintillators. *Phys. Status Solidi RRL* **2015**, *9*, 489. [CrossRef]